Two-Dimensional Halide Perovskites for Radiation Detection

Bao Xiao and Yadong Xu

1 Introduction

The demand for large-volume radiation detectors based on scintillation and semiconductor materials has triggered tremendous opportunities in the field of astronomy, high energy physics, nuclear medicine, nondestructive inspection, national security, etc. [1–3]. Depending on the detection modes, the radiation detectors can be classified into direct detection by solid-state semiconductors and indirect detection by scintillators. The former detectors directly convert photons to electrons by the semiconductor materials that are sensitive to high-energy radiation, while the scintillation detectors firstly convert high-energy radiation to ultraviolet or visible light, which can further be detected by the arrayed photodetectors.

Generally, radiation detector materials need to fulfill simultaneously several desirable properties. The direct detection semiconductor materials should possess a suitable bandgap (E_g), high resistivity (ρ), high average atomic number (Z), high mobility-lifetime product ($\mu\tau$), etc., whereas scintillation detectors should have the traits of high light yield, long-term stability, and high energy resolution. On this premise, current semiconductor detectors are mainly based on CdTe, TlBr, α-HgI_2, and $Cd_{0.9}Zn_{0.1}Te$ (CZT) [4–8], and the most commercially used scintillators are bulk crystals of NaI:Tl and CsI:Tl [9, 10]. However, each suffers from unsolved issues associated with the crystal growth, device operation conditions, or the manufacturing cost, which limits there widespread development [11]. Therefore, the quest for new detection materials is required in the field of high-energy radiation detection.

B. Xiao · Y. Xu (✉)
State Key Laboratory of Solidification Processing & Key Laboratory of Radiation Detection Materials and Devices, Ministry of Industry and Information Technology, Northwestern Polytechnical University, Xi'an, China
e-mail: fsnhxiaobao@mail.nwpu.edu.cn; xyd220@nwpu.edu.cn

W. Nie, K. (Kris) Iniewski (eds.), *Metal-Halide Perovskite Semiconductors*,
https://doi.org/10.1007/978-3-031-26892-2_9

Recently, the rapidly expanding class of halide perovskites have emerged as promising candidates for radiation detection materials, owing to their high attenuation coefficient, long carrier diffusion length and lifetime, and large mobility-lifetime product [12–14]. Compared to the degradation of the three-dimensional (3D) halide perovskite devices for long-term operations resulting from the poor air stability and ionic migration, two-dimensional (2D) halide perovskites present remarkable environmental and device stability and large Stokes shifts coupled with very broad emission, making it suitable as radiation detection materials [15, 16]. Therefore, this book chapter aims to summarize the recent research progress of 2D halide perovskite single crystals as X-ray detectors and then briefly talk about 2D halide perovskite scintillators applied in α-, β-particles, X-, and γ-ray detection.

2 Crystal Structure of 2D Halide Perovskites

Halide perovskites with the empirical formula of ABX_3 ($A = Cs^+$, MA^+, FA^+; $B = Sn^{2+}$, Pb^{2+}, Ge^{2+}; $X = Cl^-$, Br^-, I^-) are classified as 3D perovskite, in which BX_6 octahedra are corner-shared along three octahedral axes. However, the perovskites can be cut into slices from the 3D structure to a lower-dimensional layered configuration, all the way down to eventually isolated, zero-dimensional (0D) BX_6 octahedral clusters [17]. As the dimensional reduction of perovskites structure, the size restrictions, as outlined by the tolerance factor for the 3D structures, are gradually lifted. The layered 2D perovskites organized from BX_6 octahedra connected along two octahedral axes can be derived by slicing the 3D perovskites along the <100>, <110>, or <111> crystallographic planes and then inserting larger spacer cations to produce <100>-oriented, <110>-oriented, and <111>-oriented 2D perovskites, as shown in Fig. 1. The number of perovskite (inorganic) layers in 2D perovskites can be controlled by adjusting the stoichiometric ratio between A-site cations and larger spacer cations A′.

Among the three classifications, the <100>-oriented perovskites are the most widely investigated 2D layered perovskites, which can be further divided into Ruddlesden-Popper (RP) phase, Dion-Jacobson (DJ) phase, and alternating cations in the interlayer (ACI) phase depending on the larger spacer cations, with the general formulas of $A'_2A_{n-1}B_nX_{3n+1}$, $A''A_{n-1}B_nX_{3n+1}$, and $A'A_nB_nX_{3n+1}$, respectively. The spacer layer in RP perovskites is composed of two layers of monoammonium cations, which are bound to the inorganic layers from one side by hydrogen bonds (N–H•••X) between the ammonium groups and halide anions [18]. The adjacent inorganic octahedral layer misaligned by half an octahedral unit, showing a (1/2, 1/2) in-plane displacement [19]. However, for the DJ perovskites, the monoammonium cations in the organic layer are replaced by the diammonium cations that contain two amino groups at both ends connecting to the inorganic layers by hydrogen bonds (N–H•••X) [20], which leads to an eclipsed stacking of the adjacent inorganic layers exactly on top of each other with non-displacement (0, 0) [19]. The adjacent inorganic layers in ACI perovskites are eclipsed looking from *a* (or *b*)

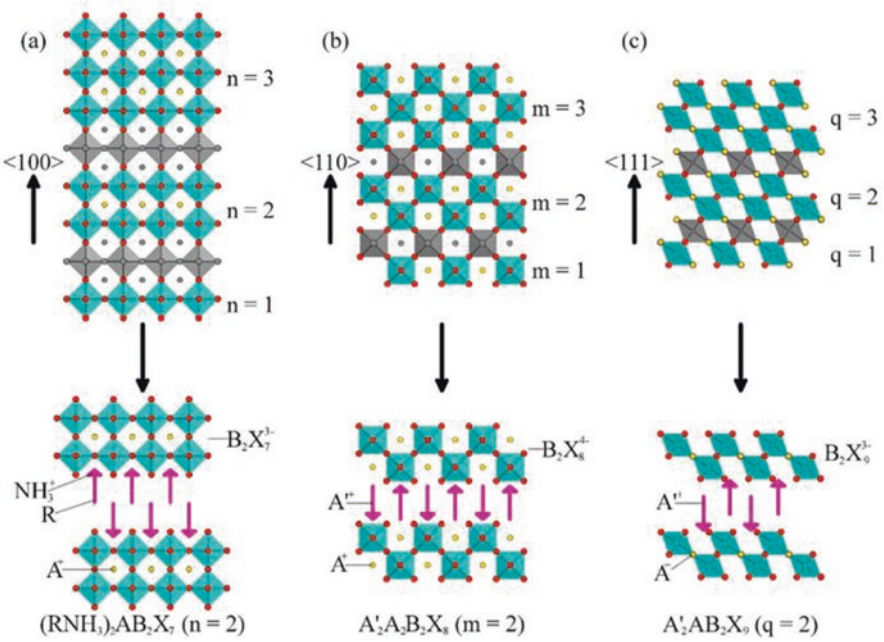

Fig. 1 Schematic representation of different families of layered perovskites: (**a**) <100>-oriented 2D perovskites with a general formula of $A'_2A_{n-1}B_nX_{3n+1}$, (**b**) <110>-oriented 2D perovskites with a general formula of $A'_2A_mB_mX_{3m+2}$, (**c**) <111>-oriented 2D perovskites with a general formula of $A'_2A_{q-1}B_qX_{3q+3}$ [24]. Reprinted with permission from Ref. [24]. Copyright 2016 American Chemical Society

direction, but staggered from *b* (or *a*) direction, leading to a (0, 1/2) or (1/2, 0) displacement [19]. Moreover, the A-site cation exists not only inside the octahedral cage but also between the layers alternating with larger organic cation (A′). To date, only the guanidinium cation can template this type of structure [21].

Compared to 3D halide perovskites, the interchangeability of the large organic cations (A′) and the control of layer dimensionality (*n*) offer 2D layered perovskites with greater structure tenability and further exhibit flexibility physical and optoelectronic properties, enabling them applied in various optoelectronic devices such as solar cells, light-emitting diodes (LED), radiation detectors, etc. [22, 23].

3 Advances in the Development of 2D Halide Perovskites X-Ray Direct Detectors

As mentioned above, the flexibility physical and optoelectronic properties of 2D halide perovskites enable them as promising candidates for radiation detectors, especially as X-ray detectors. In this section, the key parameters for X-ray direct

detection and the advances in the development of 2D halide perovskites X-ray direct detectors are systematically summarized.

3.1 The Key Parameters for X-Ray Direct Detectors

The performance of X-ray detector is largely limited by the properties of the X-ray absorber materials, which play vital roles in the processes of X-ray absorption, electron-hole pair generation, and transport. This section is aimed to introduce some key parameters for choosing X-ray detector materials and evaluating the X-ray detection performance.

(1) *The Selection of Perovskites for X-Ray Detectors.*

Stopping Power The stopping power is defined as the capability of a given material to completely absorb X-ray, which is usually quantified by the X-ray attenuation ratio (ε):

$$\varepsilon = 1 - \frac{I(x)}{I(0)} = 1 - e^{-\mu x} \tag{1}$$

where x is the material thickness and μ is the attenuation coefficient of the material, which is proportional to Z^4/E^3 (where Z is the atomic number and E is the X-ray photon energy). Thus, halide perovskite materials with high-Z elements enable them as ideal X-ray detector materials.

Ionization Energy The ionization energy ($W_{\pm}$) is defined as the energy required of the given material absorbing the X-ray to produce one free electron-hole pair, which is proportional to the energy bandgap (E_g) of the given material, and can be written as [25]:

$$W_{\pm} = 2E_g + 1.43 \tag{2}$$

Obviously, the narrower bandgap would result in a lower ionization energy ($W_{\pm}$), which is beneficial for the production of electron-hole pair in a given halide perovskite material. However, the perovskites with small bandgap also bring a large dark current and high noise. Therefore, suitable bandgap is necessary for halide perovskites operated as X-ray detectors [26].

Mobility-Lifetime Product The mobility-lifetime product ($\mu\tau$) is used to estimate the ability of charge carriers to drift before recombination in a given material and can be derived by the modified Hecht equation [27]:

$$I = \frac{I_0 \mu\tau V}{L^2} \cdot \frac{1 - \exp\left(-\frac{L^2}{\mu\tau V}\right)}{1 + \frac{L}{V} \cdot \frac{s}{\mu}} \tag{3}$$

where I and I_0 are the measured photocurrent and saturated photocurrent, respectively. L is the material thickness, V is the applied bias, and s is the surface recombination velocity. Thus, high $\mu\tau$ product directly determines the charge collection efficiency of given halide perovskites, which is essential to enhance the X-ray sensitivity.

(2) *The Key Performance Parameters for X-Ray Detectors.*

Sensitivity Sensitivity (S) is a key parameter for X-ray detectors, which reflects the ability of a detector to convert incident X-ray photons into current signals, and can be estimated by [28]:

$$S = \frac{I_p - I_d}{A \times D} \tag{4}$$

where I_p and I_d are the measured photocurrent and dark current, respectively. A is the effective area of X-ray detector and D is the dose rate. Therefore, X-ray detectors with high sensitivity can generate large current signals at a low dose rate, which is beneficial for reducing the risk of ionizing radiation [29].

Detection Limit The detection limit is another critical parameter for X-ray detectors, which determines the lowest detectable X-ray dose rate. The International Union of Pure and Applied Chemistry (IU-PAC) defines the detection limit as the equivalent dose rate to produce a signal greater than three times the noise level, so the signal-to-noise ratio (SNR) of 3 is used to define the detection limit in X-ray detectors [30]. Generally, the SNR can be calculated by:

$$SNR = \frac{I_{signal}}{I_{noise}} = \frac{I_p - I_d}{\sqrt{\frac{1}{N}\sum_{i}^{N}\left(I_i - I_p\right)^2}} \tag{5}$$

where I_{signal} and I_{noise} are the signal current and noise current, whereas I_p and I_d are the average photocurrent and dark current, respectively. A low detection limit not only allows for a reduced dose rate for X-ray examination, which significantly suppresses the risk of cancer, but also favors of high-resolution images acquisition.

Response Speed Response speed is defined as the time taken for the detector to respond to an external stimulus of detector, which is highly dependent on the carrier transport and collection processes in the detector. Therefore, the rise time (τ_r, the

time required for the current rising from 10% to 90% of the saturated photocurrent) and fall time (τ_f, the time required for the current falling from 90% to 10% of the saturated photocurrent) are often adopted to estimate the response capability of the detector. It is significant the X-ray detector should possess short response time, which can shorten the X-ray exposure time and enable higher frame rate during imaging [31].

3.2 2D Halide Perovskites X-Ray Direct Detectors

Currently, 3D halide perovskites, possessing high attenuation coefficient, long carrier diffusion length and lifetime, and large mobility-lifetime product, have shown great potential for direct X-ray detectors. However, their inherent stability (moisture, light, heat, etc.) and operational stability hinder the further applications of 3D halide perovskites in X-ray detection. 2D halide perovskites generally possess suppressed ion migration along with intrinsic chemical and moisture stability, showing more promising X-ray detection performance.

In 2019, 2D layered $(NH_4)_3Bi_2I_9$ perovskite single crystal has been proposed as X-ray direct detectors, which exhibits a unique anisotropic detection performance mainly ascribed to its anisotropic structure. For example, the $\mu\tau$ product for the direction parallel to the cleavage (001) surface is 1.1×10^{-2} $cm^2 \bullet V^{-1}$, which is almost three times than that of the direction perpendicular to (001) plane of 4.0×10^{-3} $cm^2 \bullet V^{-1}$. Consequently, the resulting parallel direction $(NH_4)_3Bi_2I_9$ detector exhibits a much higher X-ray sensitivity of 8.2×10^3 $\mu C \bullet Gy^{-1} \bullet cm^{-2}$ than the perpendicular direction detector of 803 $\mu C \bullet Gy^{-1} \bullet cm^{-2}$ due to charge transport and collection anisotropy, as shown in Fig. 2a–c. However, the perpendicular direction $(NH_4)_3Bi_2I_9$ detector exhibits a much lower X-ray detection limit of 55 $nGy \bullet s^{-1}$ than the parallel direction detector of 210 $nGy \bullet s^{-1}$, ascribed to the suppressed ion migration. Moreover, both parallel and perpendicular $(NH_4)_3Bi_2I_9$ X-ray detectors show an excellent operational stability under continuous working biases on a 10-h scale. It is highlighted that the anisotropic X-ray detection property enables $(NH_4)_3Bi_2I_9$ X-ray detector to be utilized in different practical conditions [32]. Then, centimeter-size all-inorganic 2D perovskite $Cs_3Bi_2I_6Br_3$ have been reported for X-ray detection, which shows a high sensitivity of 3194.59 $\mu C \bullet Gy^{-1} \bullet cm^{-2}$, much higher than its 0D counterpart $Cs_3Bi_2I_9$ of 707.81 $\mu C \bullet Gy^{-1} \bullet cm^{-2}$, ascribed to the enhancement of carrier transport (Fig. 2d–e). Moreover, the fabricated $Cs_3Bi_2I_6Br_3$ detector exhibits an outstanding operational stability under continuous working at a relatively high electric field [33]. By the way, both the perovskites $(NH_4)_3Bi_2I_9$ and $Cs_3Bi_2I_6Br_3$ can be considered as the derivatives ($A' = A$ and $q = 2$, i.e., $A_3B_2X_9$) by slinging the 3D perovskites along the <111> crystallographic planes, resulting in the <111>-oriented 2D perovskites.

In addition, <100>-oriented 2D Ruddlesden-Popper (RP) and Dion-Jacobson (DJ) perovskites have recently shown very promising performance in X-ray detection. For example, the insulating butylamine (BA) organic cation has been

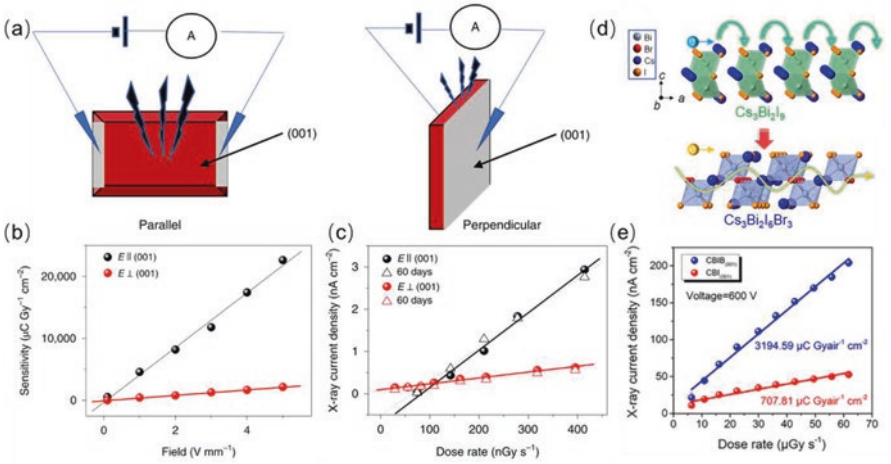

Fig. 2 (**a**) Illustration of parallel and perpendicular device structure of $(NH_4)_3Bi_2I_9$. (**b**) X-ray sensitivities of the $(NH_4)_3Bi_2I_9$ devices in direction parallel and perpendicular to the (001) surface. (**c**) Anisotropic X-ray photocurrent densities at different dose rates under pristine conditions (solid lines) and after 60 days of ambient air aging (dotted lines) [32]. Reprinted with permission from Ref. [32]. Copyright 2019 Springer Nature. (**d**) Schematic assumption of the carrier transport path in $Cs_3Bi_2I_9$ and $Cs_3Bi_2I_6Br_3$. (**e**) Electric field-dependent extracted X-ray sensitivities of $Cs_3Bi_2I_9$ and $Cs_3Bi_2I_6Br_3$ at 600 V [33]. Reprinted with permission from Ref. [33]. Copyright 2022 Elsevier

introduced into $Cs_2AgBiBr_6$ to generate a 2D layered RP perovskite $(BA)_2CsAgBiBr_7$, which could serve as the potential X-ray direct detector. The 2D $(BA)_2CsAgBiBr_7$ single crystal possesses a high resistivity of 1.5×10^{11} Ω•cm and large $\mu\tau$ product up to 1.21×10^{-3} $cm^2 \bullet V^{-1}$, which enables the fabricated detector to yield a superior X-sensitivity of 4.2 $\mu C \bullet Gy^{-1} \bullet cm^{-2}$ [34] (Fig. 3a–c). Then, Wei et al. found that introducing electron-deficient F atoms with neighbor benzene rings could enhance the supramolecular electrostatic interaction as supramolecular anchor, leading to a 2D RP perovskite 4-fluorophenethylammonium lead iodide $(F\text{-}PEA)_2PbI_4$. The fabricated $(F\text{-}PEA)_2PbI_4$ single-crystal detector yields an X-ray sensitivity of 3402 $\mu C \bullet Gy^{-1} \bullet cm^{-2}$ to 120 keVp hard X-ray with lowest detectable X-ray dose rate of 23 $nGy \bullet s^{-1}$. Moreover, the detector also exhibits excellent operation stability under ambient condition at 200 V high bias, showing stable response to hard X-ray pulses with no signal-to-noise ratio loss after over 1-month storage [35] (Fig. 3d–e).

The natural multiple quantum well (MQW) structure enables 2D RP perovskites with anisotropic X-ray detection performance. For example, the detector based on 2D $(BA)_2CsPb_2Br_7$ single crystal along *ab* plane exhibited superior X-ray sensitivity up to 13.26 $mC \bullet Gy^{-1} \bullet cm^{-2}$ at a relatively low electric field of 2.53 V mm^{-1}, while lower than 20 $\mu C \bullet Gy^{-1} \bullet cm^{-2}$ along *c* direction even at a pretty high electric field of 70 V mm^{-1} under the same irradiation of 40 kVp. However, the anisotropic detection performance could be adjusted by shortening the spacer cation from butylamine (BA) to isobutylamine (i-BA) to reduce the interlayer distance and barrier

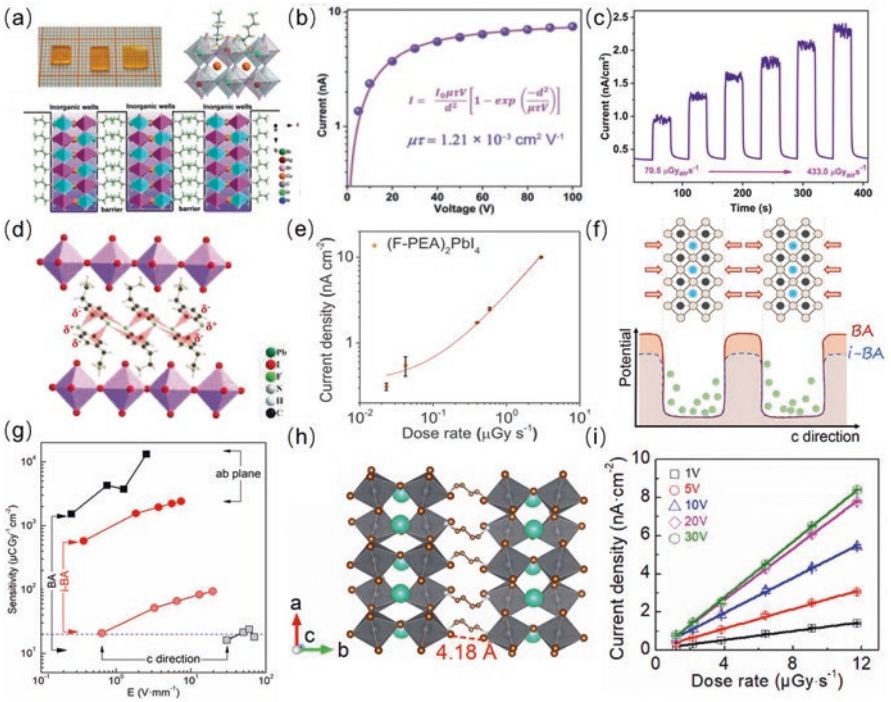

Fig. 3 (**a**) Photograph and crystal structure of $(BA)_2CsAgBiBr_7$. (**b**) Photoconductivity of single-crystalline $(BA)_2CsAgBiBr_7$. (**c**) X-ray response of $(BA)_2CsAgBiBr_7$ detector with varied dose rate [34]. Reprinted with permission from Ref. [34]. Copyright 2019 Wiley-VCH. (**d**) The crystal structure of $(F\text{-}PEA)_2PbI_4$, where electron-deficient F atoms form supramolecular electrostatic interaction with neighbor benzene rings. (**e**) The current density of $(F\text{-}PEA)_2PbI_4$ single-crystal device at different X-ray dose rates [35]. Reprinted with permission from Ref. [35]. Copyright 2020 Wiley-VCH. (**f**) Schematic diagram of charge transport restriction along the *c* direction in 2D perovskites $(BA)_2CsPb_2Br_7$ and $(i\text{-}BA)_2CsPb_2Br_7$. (**g**) Electric field-dependent X-ray sensitivities of $(BA)_2CsPb_2Br_7$ and $(i\text{-}BA)_2CsPb_2Br_7$ crystal detectors along the *ab* plane and *c* direction, respectively [36]. Reprinted with permission from Ref. [36]. Copyright 2021 Royal Society of Chemistry. (**h**) The crystal structure of $(BDA)CsPb_2Br_7$. (**i**) Dose rate-dependent current densities of $(BDA)CsPb_2Br_7$ detector under various biases [38]. Reprinted with permission from Ref. [38]. Copyright 2022 American Chemical Society

height, which resulted in lower X-ray sensitivity along *ab* plane and higher *c* direction X-ray sensitivity in 2D RP perovskite $(i\text{-}BA)_2CsPb_2Br_7$ [36] (Fig. 3f–g).

Furthermore, compared with the 2D RP perovskites, 2D Dion-Jacobson (DJ) perovskites have exhibited improved stability and electrical properties. The diammonium cations ($NH_3C_4H_8NH_3^{2+}$, BDA^{2+}) have been employed to form a 2D DJ perovskite $BDAPbI_4$, which also exhibits an excellent sensitivity of 242 $\mu C \bullet Gy^{-1} \bullet cm^{-2}$ under the 10 V bias with a detection limit as low as 430 $nGy \bullet s^{-1}$ [37]. Moreover, the diammonium cations (BDA^{2+}) have also been introduced to $CsPbBr_3$ to obtain a novel 2D DJ perovskite $(BDA)CsPb_2Br_7$, which enables the resulting detector along the out-of-plane direction to achieve a high X-ray sensitivity of 725.5 $\mu C \bullet Gy^{-1} \bullet cm^{-2}$ with excellent working stability [38] (Fig. 3h–i).

4 2D Halide Perovskite Semiconductor for Alpha Particle Detection

For the high-energy alpha particles (~3–7 MeV), the direct radiation detectors usually work in voltage mode, since the particle flux is relatively weak and alpha particles will come into the detector one by one with a shallow penetration depth. However, alpha particle is still destructive ionizing radiation, and it is very important for developing high-performance detectors for alpha particle detection. Recently, Xu et al. have developed a novel alpha detector based on a 2D DJ perovskite (BDA) $CsPb_2Br_7$ single crystal (inset in Fig. 4b). Then, a 5.48 MeV ^{241}Am α-particle source was adopted to analyze the radiation detection performance of resulting Au/(BDA) $CsPb_2Br_7$/Au device, as shown in Fig. 4a. A voltage-dependent energy spectra of (BDA)$CsPb_2Br_7$ detector with the bias changing from −100 V to −300 V can be seen in Fig. 4c. Specially, a superior energy resolution of 37% (FWHM) was achieved at −260 V bias (inset in Fig. 4c). The hole mobility-lifetime product $(\mu\tau)_h$ could be evaluated using the single charge carrier approximation Hecht equation [39]:

$$CCE = \frac{\mu\tau V}{d^2} \cdot \left(1 - \exp\left(-\frac{d^2}{\mu\tau V}\right)\right) \tag{6}$$

Therefore, the hole mobility-lifetime product $(\mu\tau)_h$ of (BDA)$CsPb_2Br_7$ crystal was calculated to be $(2.33 \pm 0.08) \times 10^{-5}$ $cm^2 \cdot V^{-1}$ by fitting the peak centroid channel vs. the bias voltage using Eq. (3), as shown in Fig. 4d [38]. The results suggest that the 2D DJ perovskite (BDA)$CsPb_2Br_7$ could serve as the potential alpha particle-detecting material.

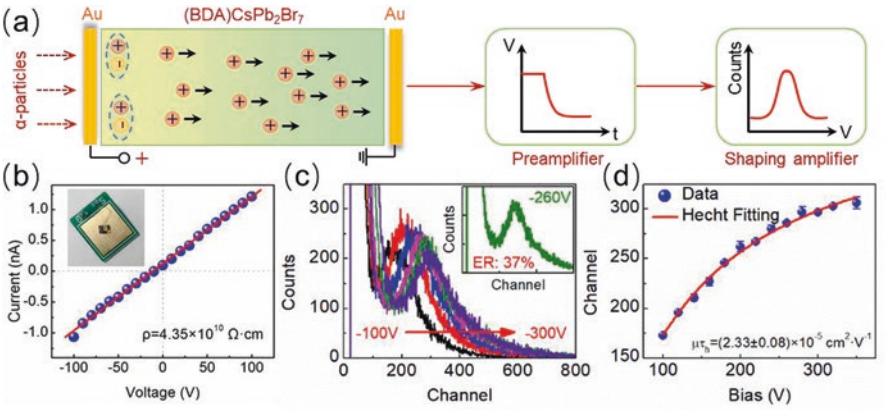

Fig. 4 (**a**) Hole transport process in Au/(BDA)$CsPb_2Br_7$/Au device illuminated by ^{241}Am α-particles. (**b**) The typical I-V curve of (BDA)$CsPb_2Br_7$; the inset is the fabricated Au/(BDA) $CsPb_2Br_7$/Au detector. (**c**) The energy spectra of (BDA)$CsPb_2Br_7$ detector under various voltages, respectively. The inset is the typical energy spectra under −260 V with a resolution of 37%. (**d**) The hole mobility-lifetime product evaluation of (BDA)$CsPb_2Br_7$ according to the Hecht equation [38]. Reprinted with permission from Ref. [38]. Copyright 2022 American Chemical Society

5 Advances in the Development of 2D Halide Perovskite Scintillators for Radiation Detection

The scintillation detectors are also capable of detecting high-energy particles or photons by indirect detection mode. Generally, the scintillation detectors firstly convert high-energy radiation to ultraviolet or visible light, which can further be detected by the arrayed photodetectors. Light yield (LY) and decay time are the most important figures of merit for scintillation detectors. LY indicates the number of photons that can be converted by the scintillator per photon or particle energy (in unit) and can be calculated by:

$$LY = 10^6 \frac{SQ}{\beta E_g} \tag{7}$$

where S is the efficiency of the transport of electron-hole pairs to the emission center, Q is the luminescence efficiency, and β is usually a constant with a value of 2.5. A high LY value indicates the high number of photons emitted from the scintillator which leads to a high signal output. It is generally believed that 2D perovskites are able to show high scintillation light yield and faster decay due to their higher exciton binding energy (hundreds of meV) [40]. In this section, the advances in the development of 2D halide perovskite scintillators are systematically summarized.

5.1 Alpha Particle Detectors

Developing high-performance detectors for alpha particle is important for environmental safety. Recently, lithium-doped 2D RP perovskite $(PEA)_2PbBr_4$ has been synthesized for multiple radiation detectors and scintillators for the first time (Fig. 5a). With a lithium dopant, the 1:1 Li-doped $(PEA)_2PbBr_4$ scintillator demonstrated a fast decay time of 11 ns and a high scintillation yield light of 11,000 photons per MeV (Fig. 5b). Figure 5c shows the pulse-height spectra results of the Li-doped $(PEA)_2PbBr_4$ scintillator using ^{241}Am and ^{224}Cm as the alpha particle sources [41].

5.2 Beta Particle Detectors

Beta particle with a moderate penetrating power is an important signal for surface radiative contamination surveillance. In general, the incident β-particles go through elastic scattering with nuclei and inelastic scattering with electrons in solids. Currently β-particle detectors are mainly based on the organic scintillators, including single crystal, liquid, and plastic types, which was limited by the issues of high

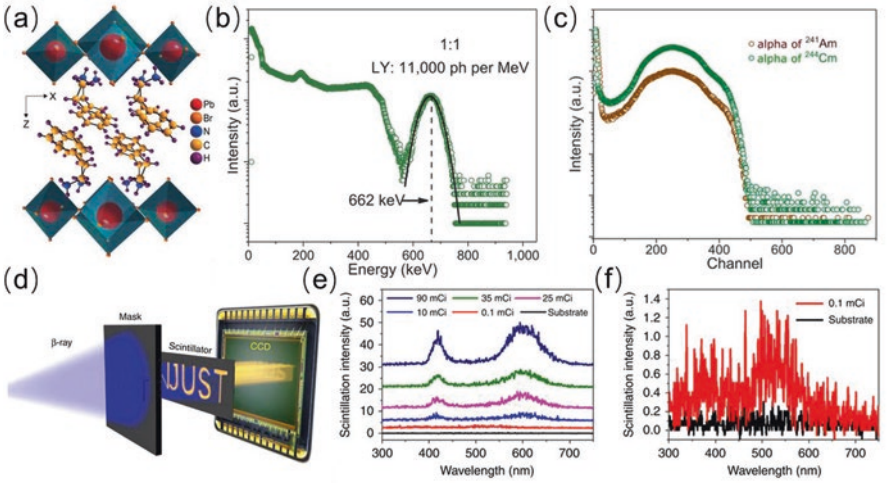

Fig. 5 (**a**) Crystal structure of $(PEA)_2PbBr_4$. (**b**) Pulse-height spectra of Li-doped $(PEA)_2PbBr_4$ with Gaussian fitting to extract light yield. (**c**) Alpha particle pulse-height spectra of Li-doped $(PEA)_2PbBr_4$ scintillator [41]. Reprinted with permission from Ref. [41]. Copyright 2020 Spring Nature. (**d**) Illustration of the setup of the system for β-particle detection by the 2D perovskite scintillator. (**e**) The scintillation spectra of the 2D perovskite scintillator under different β-particle irradiation intensity. (**f**) The scintillation spectrum under the irradiation activity of 0.1 mCi [42]. Reprinted with permission from Ref. [42]. Copyright 2020 Spring Nature

cost, poor irradiation hardness, carcinogenicity, complex fabrication, or thermal deterioration.

Recently, a type of β-particle scintillator with good thermotolerance and irradiation hardness based on 2D RP perovskites has been proposed by Zeng et al. A series of bulky organic cations in 2D RP perovskite $(A)_2PbBr_4$ (A = butylamine, BA; octylamine, OA; stearamine, STA; and dodecylamine, DA) have been explored to enhance the capturing of β-particle. Additionally, extrinsic manganese (Mn) dopants were adopted to improve the scintillation performance via serving as emitting centers with no self-absorption. Figure 5d shows the setup of the system for the β-particle detection by the 2D perovskite scintillator. The resultant 2D perovskite scintillator exhibited an effective β-particle detection performance with no functionality decay or hysteresis under an accumulated radiation dose of 10 kGy (dose rate 0.67 kGy•h^{-1}) and exhibited a low detection limit of 0.1 mCi (Fig. 5e–f) [42].

5.3 Gamma-Ray Detectors

Gamma-rays, as a form of electromagnetic waves, have the shortest wavelength and the highest energy and are usually emitted from atomic nuclei. 2D perovskite scintillator also exhibits good potential as γ-ray detection material. For example, Dang

et al. have investigated the scintillation properties from 11 different 2D organic-inorganic hybrid perovskites and found that the 3 2D perovskite $(PEA)_2PbBr_4$, $(EDBE)_2PbBr_4$, and $(BA)_2PbBr_4$ crystals have the higher light yield. Specially, $(BA)_2PbBr_4$ scintillator exhibits the highest light yield and 3.7 times greater than that of $(PEA)_2PbBr_4$ (~40,000 photons per MeV at RT), as well as being more stable from 10 K to 350 K compared to other 2D scintillators. In conjunction with the 5.3 ns fast decay time, $(BA)_2PbBr_4$ scintillator shows the energy resolution as low as 13% to resolve the 662 keV ^{137}Cs γ-ray, suggesting it can be a potential superior scintillator detector. Furthermore, Li-doped $(PEA)_2PbBr_4$ scintillator exhibits the light yield 2.009 times higher than that of undoped $(PEA)_2PbBr_4$ scintillator and achieves the best energy resolution of 7.7% at 662 keV from the ^{137}Cs γ-ray source for Li-doped $(PEA)_2PbBr_4$ scintillator [43, 44].

5.4 Neutron Detectors

A fast neutron has strong penetration ability through dense and bulky objects, which makes it an ideal nondestructive technology for detecting voids, cracks, or other defects inside large equipment. Recently, a hydrogen-rich 2D perovskite Mn-$(C_{18}H_{37}NH_3)_2PbBr_4$ (Mn-STA_2PbBr_4) has been demonstrated as fast neutron scintillator detector, where the hydrogen-rich long-chain organic amine ions lead to a high capturing efficiency of fast neutrons, and the Mn^{2+} dopants as the emitting centers improve the optical performance with no self-absorption (Fig. 6d). The fabricated large-area self-standing fast neutron scintillator plates based on 2D perovskite Mn-STA_2PbBr_4 deliver high light yields and good spatial resolution (0.5 lp/mm (lp, line pairs)), as shown in Fig. 6e–i [45]. The results open up a new route for the design of fast neutron scintillator materials and promote the development of fast neutron radiography-based nondestructive testing technologies.

6 Conclusion

In summary, the rise of halide perovskites as promising candidates for radiation detection materials has been witnessed from recent reports. Compared to the well-studied three-dimensional (3D) halide perovskite, two-dimensional (2D) halide perovskites could be obtained by slicing the 3D perovskites along different crystallographic planes with larger insulating organic cations to generate <100>-oriented, <110>-oriented, and <111>-oriented 2D perovskites, respectively. 2D layered perovskites with remarkable environmental and device stability have been reported to exhibit good potential in high-energy radiation detection in two types, namely, direct semiconductor detector and indirect scintillator detector.

The 2D perovskites have recently shown very promising performance in X-ray detection as a direct semiconductor detector. For example, the detector based on

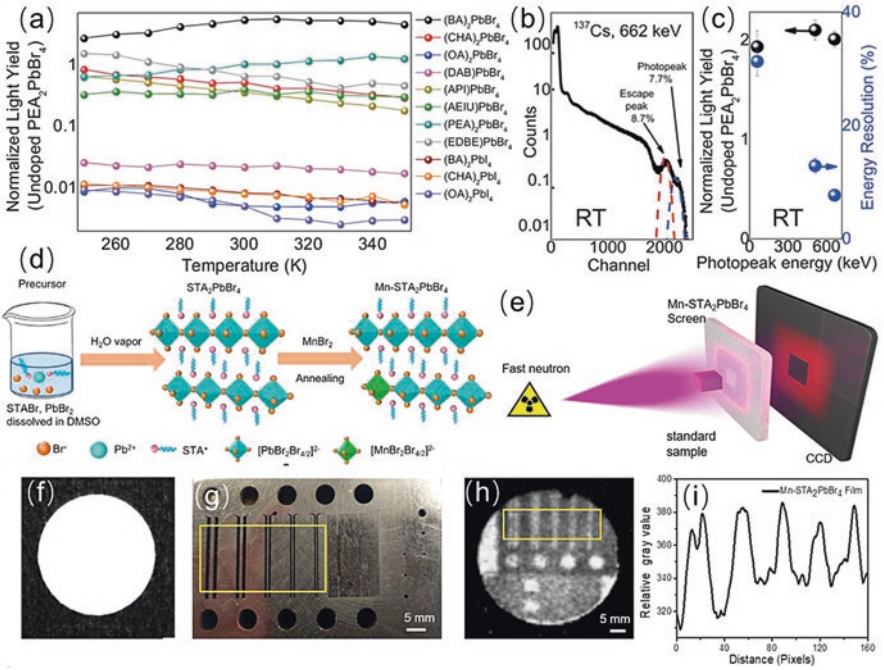

Fig. 6 (**a**) Temperature-dependent light yield of 2D perovskite for temperature between 250 and 350 K. (**b**) Pulse-height spectra of Li-doped $(PEA)_2PbBr_4$ under 662 keV gamma-ray from the ^{137}Cs source. (**c**) Light yield and energy resolution as a function of photopeak energies for different gamma-ray sources of ^{241}Am, ^{22}Na, and ^{137}Cs. The y-axis is normalized with the light yields of undoped $(PEA)_2PbBr_4$ under 662 keV gamma-ray at RT [43]. Reprinted with permission from ref. 43. Copyright 2020 American Chemical Society. (**d**) Synthesis scheme of Mn-STA_2PbBr_4. (**e**) Schematic of the experimental setup used for fast neutron radiography of a resolution test standard sample. The sample is placed between the fast neutron source and the Mn-STA_2PbBr_4 screen. (**f**) Fast neutron radiograph is generated by a 1 mm thick Mn-STA_2PbBr_4 plate. (**g**) Resolution test standard sample (steel plate with slits, holes of different depths). (**h**) Fast neutron imaging of resolution test standard sample. Each frame of the image is exposed for 100 s under a 14 MeV fast neutron accelerator for a total of 20 times. (**i**) Curve of the relative gray value distribution of (**h**), which can distinguish the fissure evidently [45]. Reprinted with permission from Ref. [45]. Copyright 2021 American Chemical Society

$(BA)_2CsPb_2Br_7$ single crystal along *ab* plane exhibited superior X-ray sensitivity up to 13.26 $mC•Gy^{-1}•cm^{-2}$ at a relatively low electric field of 2.53 V mm^{-1}. The natural multiple quantum well structure enables 2D perovskite detectors with anisotropic detection performance, which can be adjusted by shortening the spacer cation to reduce the interlayer distance and barrier height. The anisotropic X-ray detection property enables 2D perovskite to be utilized in different practical conditions. Except for the semiconductor detector, 2D perovskite scintillator detectors have also exhibited excellent performance in α-, β-particles, neutron, and γ-ray detection. For example, a type of 2D perovskite scintillator was developed to detect β-ray with good thermotolerance and irradiation hardness. Li-doped $(PEA)_2PbBr_4$ scintillator

was demonstrated to resolve 662 keV γ-rays with an energy resolution of 7.7% and has been proven to be useful in neutron detection through ^{6}Li enrichment. Although 2D perovskites have been proven to have good potential applied in high-energy radiation detection, the properties are still to be improved for producing better 2D perovskite semiconductor detector or scintillator detector.

Acknowledgments This work was supported by the National Natural Science Foundations of China (No. 51872228, 51802262, and U2032170), the Natural Science Foundation of Shaanxi Province (2020JC-12), and the Natural Science Basic Research Plan in Shaanxi Province of China (2019ZDLGY04-07).

References

1. Owens, A., & Peacock, A. (2004). Compound semiconductor radiation detectors. *Nuclear Instruments and Methods in Physics Research Section A: Accelerators, Spectrometers, Detectors and Associated Equipment, 531*(1–2), 18–37.
2. Szeles, C. (2004). CdZnTe and CdTe materials for X-ray and gamma ray radiation detector applications. *Physica Status Solidi B: Basic Solid State Physics, 241*(3), 783–790.
3. Kim, Y. C., Kim, K. H., Son, D. Y., Jeong, D. N., Seo, J. Y., Choi, Y. S., Han, I. T., Lee, S. Y., & Park, N. G. (2017). Printable organometallic perovskite enables large-area, low-dose X-ray imaging. *Nature, 550*(7674), 87–91.
4. Schlesinger, T. E., Toney, J. E., Yoon, H., Lee, E. Y., Brunett, B. A., Franks, L., & James, R. B. (2001). Cadmium zinc telluride and its use as a nuclear radiation detector material. *Materials Science and Engineering R, 32*(4), 103–189.
5. Locker, M., Fischer, P., Krimmel, S., Kruger, H., Lindner, M., Nakazawa, K., Takahashi, T., & Wermes, N. (2004). Single photon counting X-ray imaging with Si and CdTe single chip pixel detectors and multichip pixel modules. *IEEE Transactions on Nuclear Science, 51*(4), 1717–1723.
6. Melnikov, A. (1999). CdZnTe radiation detectors. *Journal of Crystal Growth, 197*(3), 663–665.
7. Gits, S., & Authier, A. (1982). Plastic defects in α-HgI_2 single crystals. *Journal of Crystal Growth, 58*(3), 473–485.
8. Hitomi, K., Onodera, T., & Shoji, T. (2007). Influence of zone purification process on TlBr crystals for radiation detector fabrication. *Nuclear Instruments and Methods in Physics Research Section A: Accelerators, Spectrometers, Detectors and Associated Equipment, 579*(1), 153–156.
9. Moszyński, M., Zalipska, J., Balcerzyk, M., Kapusta, M., Mengesha, W., & Valentine, J. D. (2002). Intrinsic energy resolution of NaI(Tl). *Nuclear Instruments and Methods in Physics Research Section A: Accelerators, Spectrometers, Detectors and Associated Equipment, 484*(1), 259–269.
10. Nagarkar, V. V., Gupta, T. K., Miller, S. R., Klugerman, Y., Squillante, M. R., & Entine, G. (1998). Structured CsI(Tl) scintillators for X-ray imaging applications. *IEEE Transactions on Nuclear Science, 45*(3), 492–496.
11. Owens, A. (2006). Semiconductor materials and radiation detection. *Journal of Synchrotron Radiation, 13*(2), 143–150.
12. Dong, Q., Fang, Y., Shao, Y., Mulligan, P., Qiu, J., Cao, L., & Huang, J. (2015). Electron-hole diffusion lengths>175 μm in solution-grown $CH_3NH_3PbI_3$ single crystals. *Science, 347*(6225), 967–970.
13. McMeekin, D. P., Sadoughi, G., Rehman, W., Eperon, G. E., Saliba, M., Hörantner, M. T., Haghighirad, A., Sakai, N., Korte, L., Rech, B., Johnston, M. B., Herz, L. M., & Snaith,

H. J. (2016). A mixed-cation lead mixed-halide perovskite absorber for tandem solar cells. *Science, 351*(6269), 151–155.
14. Shi, D., Adinolfi, V., Comin, R., Yuan, M., Alarousu, E., Buin, A., Chen, Y., Hoogland, S., Rothenberger, A., Katsiev, K., Losovyj, Y., Zhang, X., Dowben, P. A., Mohammed, O. F., Sargent, E. H., & Bakr, O. M. (2015). Low trap-state density and long carrier diffusion in organolead trihalide perovskite single crystals. *Science, 347*(6221), 519–522.
15. Smith, I. C., Hoke, E. T., Solisibarra, D., Mcgehee, M. D., & Karunadasa, H. I. (2014). A layered hybrid perovskite solar-cell absorber with enhanced moisture stability. *Angewandte Chemie, International Edition, 53*(42), 11232–11235.
16. Lin, Y., Bai, Y., Fang, Y., Wang, Q., Deng, Y., & Huang, J. (2017). Suppressed ion migration in low-dimensional perovskites. *ACS Energy Letters, 2*(7), 1571–1572.
17. Saidaminov, M. I., Mohammed, O. F., & Bakr, O. M. (2017). Low-dimensional-networked metal halide perovskites: The next big thing. *ACS Energy Letters, 2*(4), 889–896.
18. Stoumpos, C. C., Cao, D. H., Clark, D. J., Young, J., Rondinelli, J. M., Jang, J. I., Hupp, J. T., & Kanatzidis, M. G. (2016). Ruddlesden-Popper hybrid lead iodide perovskite 2D homologous semiconductors. *Chemistry of Materials, 28*(8), 2852–2867.
19. Blancon, J. C., Even, J., Stoumpos, C. C., Kanatzidis, M. G., & Mohite, A. D. (2020). Semiconductor physics of organic-inorganic 2D halide perovskites. *Nature Nanotechnology, 15*(12), 969–985.
20. Li, X., Hoffman, J., Ke, W., Chen, M., Tsai, H., Nie, W., Mohite, A. D., Kepenekian, M., Katan, C., Even, J., Wasielewski, M. R., Stoumpos, C. C., & Kanatzidis, M. G. (2018). Two-dimensional halide perovskites incorporating straight chain symmetric diammonium ions, $(NH_3C_mH_{2m}NH_3)(CH_3NH_3)_{n-1}Pb_nI_{3n+1}$ (m= 4-9; n= 1-4). *Journal of the American Chemical Society, 140*(38), 12226–12238.
21. Soe, C. M. M., Stoumpos, C. C., Kepenekian, M., Traoré, B., Tsai, H., Nie, W., Wang, B., Katan, C., Seshadri, R., & Mohite, A. D. (2017). New type of 2D perovskites with alternating cations in the interlayer space, $(C(NH_2)_3)(CH_3NH_3)_nPb_nI_{3n+1}$: Structure, properties, and photovoltaic performance. *Journal of the American Chemical Society, 139*(45), 16297–16309.
22. Chen, P., Bai, Y., Lyu, M., Yun, J.-H., Hao, M., & Wang, L. (2018). Progress and perspective in low-dimensional metal halide perovskites for optoelectronic applications. *Solar RRL, 2*(3), 1700186.
23. Wong, J., & Yang, K. (2021). 2D hybrid halide perovskites: Synthesis, properties, and applications. *Solar RRL, 5*(1), 2000395.
24. Saparov, B., & Mitzi, D. B. (2016). Organic-inorganic perovskites: Structural versatility for functional materials design. *Chemical Reviews, 116*(7), 4558–4596.
25. Devanathan, R., Corrales, L. R., Gao, F., & Weber, W. J. (2006). Signal variance in gamma-ray detectors – A review. *Nuclear Instruments and Methods in Physics Research Section A: Accelerators, Spectrometers, Detectors and Associated Equipment, 565*(2), 637–649.
26. Li, Z., Zhou, F., Yao, H., Ci, Z., Yang, Z., & Jin, Z. (2021). Halide perovskites for high-performance X-ray detector. *Materials Today, 48*, 155–175.
27. Stoumpos, C. C., Malliakas, C. D., Peters, J. A., Liu, Z., Sebastian, M., Im, J., Chasapis, T. C., Wibowo, A. C., Chung, D. Y., Freeman, A. J., Wessels, B. W., & Kanatzidis, M. G. (2013). Crystal growth of the perovskite semiconductor $CsPbBr_3$: A new material for high-energy radiation detection. *Crystal Growth & Design, 13*(7), 2722–2727.
28. Kasap, S. (2000). X-ray sensitivity of photoconductors: Application to stabilized a-Se. *Journal of Physics D: Applied Physics, 33*(21), 2853–2865.
29. Wei, H., Fang, Y., Mulligan, P., Chuirazzi, W., Fang, H.-H., Wang, C., Ecker, B. R., Gao, Y., Loi, M. A., Cao, L., & Huang, J. (2016). Sensitive X-ray detectors made of methylammonium lead tribromide perovskite single crystals. *Nature Photonics, 10*(5), 333–339.
30. Thompson, M., Ellison, S. L., & Wood, R. (2002). Harmonized guidelines for single-laboratory validation of methods of analysis (IUPAC Technical Report). *Pure and Applied Chemistry, 74*(5), 835–855.

31. Kakavelakis, G., Gedda, M., Panagiotopoulos, A., Kymakis, E., Anthopoulos, T. D., & Petridis, K. (2020). Metal halide perovskites for high-energy radiation detection. *Advancement of Science, 7*(22), 2002098.
32. Zhuang, R., Wang, X., Ma, W., Wu, Y., Chen, X., Tang, L., Zhu, H., Liu, J., Wu, L., Zhou, W., Liu, X., & Yang, Y. (2019). Highly sensitive X-ray detector made of layered perovskite-like $(NH_4)_3Bi_2I_9$ single crystal with anisotropic response. *Nature Photonics, 13*(9), 602–608.
33. Sun, Q., Xiao, B., Ji, L., Zhao, D., Liu, J., Zhang, W., Zhu, M., Jie, W., Zhang, B.-B., & Xu, Y. (2022). Effect of dimensional expansion on carrier transport behaviors of the hexagonal Bi-based perovskite crystals. *Journal of Energy Chemistry, 66*, 459–465.
34. Xu, Z., Liu, X., Li, Y., Liu, X., Yang, T., Ji, C., Han, S., Xu, Y., Luo, J., & Sun, Z. (2019). Exploring lead-free hybrid double perovskite crystals of $(BA)_2CsAgBiBr_7$ with large mobility-lifetime product toward X-ray detection. *Angewandte Chemie, International Edition, 58*(44), 15757–15761.
35. Li, H., Song, J., Pan, W., Xu, D., Zhu, W.-A., Wei, H., & Yang, B. (2020). Sensitive and stable 2D perovskite single-crystal X-ray detectors enabled by a supramolecular anchor. *Advanced Materials, 32*(40), 2003790.
36. Xiao, B., Sun, Q., Wang, F., Wang, S., Zhang, B., Wang, J., Jie, W., Sellin, P., & Xu, Y. (2021). Towards superior X-ray detection performance of two-dimensional halide perovskite crystals by adjusting anisotropic transport behavior. *Journal of Materials Chemistry A, 9*(22), 13209–13219.
37. Shen, Y., Liu, Y., Ye, H., Zheng, Y., Wei, Q., Xia, Y., Chen, Y., Zhao, K., Huang, W., & Liu, S. (2020). Centimeter-sized single crystal of two-dimensional halide perovskites incorporating straight chain symmetric diammonium ion for efficient X-ray detection. *Angewandte Chemie, International Edition, 59*(35), 14896–14902.
38. Xiao, B., Sun, Q., Wang, S., Ji, L., Li, Y., Xi, S., Zhang, B.-B., Wang, J., Jie, W., & Xu, Y. (2022). Two-dimensional Dion-Jacobson perovskite $(NH_3C_4H_8NH_3)CsPb_2Br_7$ with high X-ray sensitivity and peak discrimination of α-particles. *Journal of Physical Chemistry Letters, 13*(5), 1187–1193.
39. Sellin, P. J., Davies, A. W., Gkoumas, S., Lohstroh, A., Özsan, M. E., Parkin, J., Perumal, V., Prekas, G., & Veale, M. (2008). Ion beam induced charge imaging of charge transport in CdTe and CdZnTe. *Nuclear Instruments and Methods in Physics Research Section B: Beam Interactions with Materials and Atoms, 266*(8), 1300–1306.
40. Blancon, J. C., Stier, A. V., Tsai, H., Nie, W., Stoumpos, C. C., Traoré, B., Pedesseau, L., Kepenekian, M., Katsutani, F., Noe, G. T., Kono, J., Tretiak, S., Crooker, S. A., Katan, C., Kanatzidis, M. G., Crochet, J. J., Even, J., & Mohite, A. D. (2018). Scaling law for excitons in 2D perovskite quantum wells. *Nature Communications, 9, (1)*, 2254.
41. Xie, A., Hettiarachchi, C., Maddalena, F., Witkowski, M. E., Makowski, M., Drozdowski, W., Arramel, A., Wee, A. T. S., Springham, S. V., Vuong, P. Q., Kim, H. J., Dujardin, C., Coquet, P., Birowosuto, M. D., & Dang, C. (2020). Lithium-doped two-dimensional perovskite scintillator for wide-range radiation detection. *Communications Materials, 1*(1), 37.
42. Yu, D., Wang, P., Cao, F., Gu, Y., Liu, J., Han, Z., Huang, B., Zou, Y., Xu, X., & Zeng, H. (2020). Two-dimensional halide perovskite as β-ray scintillator for nuclear radiation monitoring. *Nature Communications, 11*(1), 3395.
43. Xie, A., Maddalena, F., Witkowski, M. E., Makowski, M., Mahler, B., Drozdowski, W., Springham, S. V., Coquet, P., Dujardin, C., Birowosuto, M. D., & Dang, C. (2020). Library of two-dimensional hybrid lead halide perovskite scintillator crystals. *Chemistry of Materials, 32*(19), 8530–8539.
44. Maddalena, F., Xie, A., Arramel, Witkowski, M. E., Makowski, M., Mahler, B., Drozdowski, W., Mariyappan, T., Springham, S. V., Coquet, P., Dujardin, C., Birowosuto, M. D., & Dang, C. (2021). Effect of commensurate lithium doping on the scintillation of two-dimensional perovskite crystals. *Journal of Materials Chemistry C, 9*(7), 2504–2512.
45. Zheng, J., Zeng, Y., Wang, J., Sun, C., Tang, B., Wu, Y., Zhang, Y., Yi, Y., Wang, N., Zhao, Y., & Zhou, S. (2021). Hydrogen-rich 2D halide perovskite scintillators for fast neutron radiography. *Journal of the American Chemical Society, 143*(50), 21302–21311.